ALKALI/TX(SUB 2) CATALYSTS FOR CO/H(SUB 2) CONVERSION TO C(SUB 1)-C(SUB 4) ALCOHOLS. TECHNICAL PROGRESS REPORT, SEPTEMBER-NOVEMBER 1990

LEHIGH UNIV.
BETHLEHEM, PA

DEC 1990

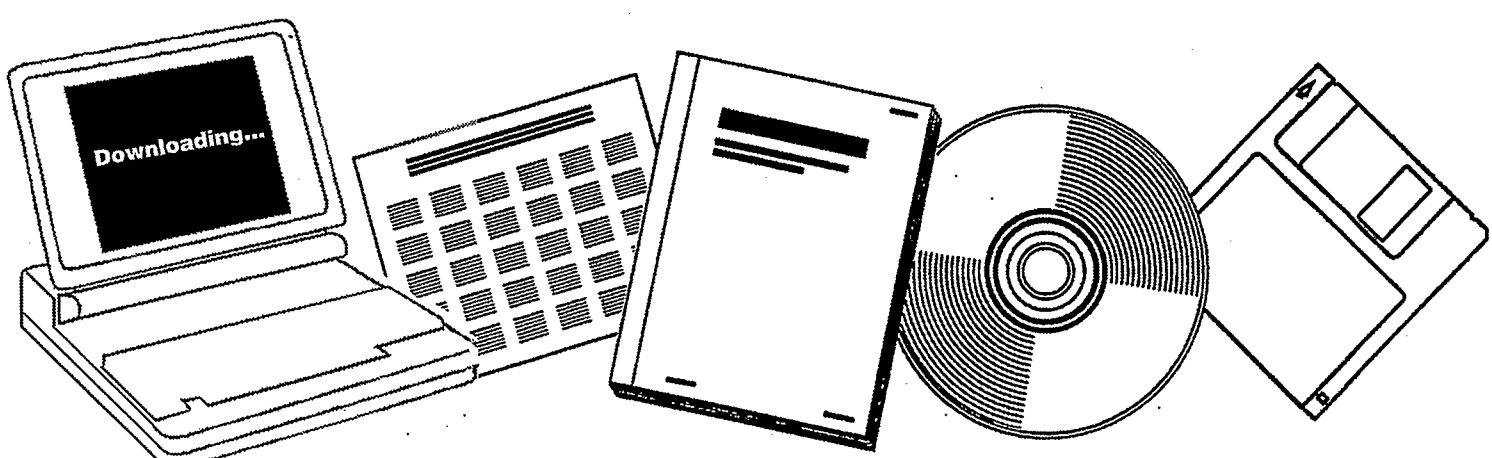

One Source. One Search. One Solution.

NTIS

Providing Permanent, Easy Access to U.S. Government Information

National Technical Information Service is the nation's largest repository and disseminator of government-initiated scientific, technical, engineering, and related business information. The NTIS collection includes almost 3,000,000 information products in a variety of formats: electronic download, online access, CD-ROM, magnetic tape, diskette, multimedia, microfiche and paper.

Search the NTIS Database from 1990 forward

NTIS has upgraded its bibliographic database system and has made all entries since 1990 searchable on **www.ntis.gov.** You now have access to information on more than 600,000 government research information products from this web site.

Link to Full Text Documents at Government Web Sites

Because many Government agencies have their most recent reports available on their own web site, we have added links directly to these reports. When available, you will see a link on the right side of the bibliographic screen.

Download Publications (1997 - Present)

NTIS can now provides the full text of reports as downloadable PDF files. This means that when an agency stops maintaining a report on the web, NTIS will offer a downloadable version. There is a nominal fee for each download for most publications.

For more information visit our website:

www.ntis.gov

U.S. DEPARTMENT OF COMMERCE
Technology Administration
National Technical Information Service
Springfield, VA 22161

DOE/PC/88933--8

DE91 005726

ALKALI/TX_2 CATALYSTS FOR CO/H_2 CONVERSION TO C_1-C_4 ALCOHOLS

Technical Progress Report for the Period

September-November 1990

Kamil Klier
and
Richard G. Herman
with
Michelle Richards and Mark Kieke

Zettlemoyer Center for Surface Studies
and Department of Chemistry
Lehigh University
Bethlehem, PA 18015

December 1990

PREPARED FOR THE UNITED STATES
DEPARTMENT OF ENERGY

Under Contract No. DE-FG22-88PC88933

ALKALI/TX_2 CATALYSTS FOR CO/H_2 CONVERSION TO C_1-C_4 ALCOHOLS

ALKALI/TX_2 CATALYSTS FOR CO/H_2 CONVERSION TO C_1-C_4 ALCOHOLS

SUMMARY OF TECHNICAL PROGRESS

New preparations of RuS_2 catalysts have been prepared using $RuCl_3$ and Li_2S reactants in methanolic solution. These catalysts have been characterized by elemental analysis, XRD, and BET surface area measurements. The elemental analysis of this catalyst gave a sulfur to ruthenium mole ratio of 2.11. XRD of the pretreated form of this catalyst showed diffraction lines due to mainly RuS_2 and only a small amount of Ru(0). BET measurement of the same sample gave a surface area of 7.0 m^2/g .

Thermodynamic calculations on the stability of the TS_2 compounds under reactor conditions have been extended to other sulfides to check for periodic trends. The stability of the TS_2 compound toward its corresponding metal, T, has been calculated. Reduction of TS_2 by the reactant gas H_2 would result in the formation of bulk metal, T. The stability of the TS_2 compound toward its corresponding oxide has also been calculated. Oxidation of the TS_2 by any H_2O present in the reactor would result in the formation of the corresponding transition metal oxide, T_xO_y. When these two tests for stability are used the sulfides found to be most stable under reactor conditions are the following: MoS_2, WS_2 and RuS_2.

The angle resolved ESCA study of a natural crystal of MoS_2 has been repeated using a conventional Mg K_α anode. This study is being carried out to differentiate diffraction peaks from forward focused peaks in the Area Mo 3d vs. polar angle graphs at constant azimuthal angle. Preliminary use of the Bragg equation indicates that peaks at polar angles of 16°, 32° and 48° obtained using Al K_α radiation will be shifted to corresponding polar angles of 19°, 39° and 62° using Mg K_α radiation.

Attempts were made to prepared niobium disulfide by three different methods. The products were characterized by XRD and elemental analyses, and all nobium sulfide preparations have resulted in substoichiometric quantities of sulfur in the compounds.

TECHNICAL PROGRESS

A. Ruthenium Disulfide Catalysts

Discussion of Thermodynamic Stability

The stability of the TX_2 catalysts under reactor conditions is very important. Thermodynamic calculations can be used to predict the stability of the TX_2 compounds toward reduction and oxidation. In the reactor, H_2 gas is present as one of the reactants present in the synthesis gas used for higher alcohol synthesis over these catalysts. The water gas shift reaction (Reaction 1) and production of hydrocarbons (Reaction 2) are both reactions that will produce H_2O in the reactor. The stability of the catalyst toward its corresponding metal and most stable oxide form can be calculated from available thermodynamic data.[1-3]

$$CO_2(g) + H_2(g) \rightarrow CO(g) + H_2O(g) \quad \Delta G(298K) = 6.683 \text{ kcal/mole} \qquad (1)$$

$$CO(g) + 3H_2(g) \rightarrow CH_4(g) + H_2O(g) \quad \Delta G(298K) = -33.97 \text{ kcal/mole} \qquad (2a)$$

$$\text{General Equation: } nCO(g) + (2n+1)H_2(g) \rightarrow C_nH_{2n+1}(g) + nH_2O(g) \qquad (2b)$$

The overall reaction for the reduction of transition metal disulfides by H_2 to the corresponding metal and H_2S is shown in Equation 3. Calculated Gibbs free energies at 298K and 1 atm pressure are given in Table 1. The most stable TS_2 compound will be the one with the most positive ΔG. One precaution must be observed when comparing these numbers. The thermodynamics discussed are bulk thermodynamic properties. The surface thermodynamics, where catalysis occurs, may be very different due to dangling bonds and unshared valencies. Of the layer compounds, NbS_2 has the most positive free energy for reduction to its metal. For the pyrite compounds, RuS_2 is the most stable toward reduction. The general trend in

layer compounds is a decrease in stability as one proceeds across and down the periodic table (order of stability: Nb > Ta > Mo > W > Tc > Re). Pyritic compounds seem to decrease in stability as one proceeds across the periodic table as well (order of stability: Mn > Ru > Fe > Co > Os > Ni).

$$TS_2(s) + 2H_2(g) \rightarrow T(s) + 2H_2S(g) \qquad (3)$$

TABLE 1

Calculated Gibbs Free Energy (kcal/mode) for Reaction 3 at 298K and 1 atm for the Transition Metal Sulfides as a Function of Position in the Periodic Table.[1-3]

VB	VIB	VIIB	VIII	VIII	VIII
----	----	MnS_2(37.8)	FeS_2(22.3)	CoS_2(18.8)	NiS_2(14.1)
NbS_2(66.8)	MoS_2(47.7)	TcS_2(35.7)	RuS_2(30.5)	----	----
TaS_2(66.5)	WS_2(43.8)	ReS_2(23.9)	OsS_2(16.3)	----	----

When the stability of the TS_2 compounds are compared to the corresponding stable oxide forms (Table 2), the trend is markedly different. The general overall reaction is shown in Equation 4 and the calculated Gibbs

$$MS_2(s) + (y/x)\ H_2O(g) \rightarrow (1/x)\ M_xO_y(s) + 2\ H_2S(g) + (y/(x-2))\ H_2(g) \qquad (4)$$

free energy values at 298 K and 1 atm pressure are given in Table 3. In general the trend is opposite to that found for the corresponding reduction, as represented by Equation 3. The layer compounds increase in stability as one proceeds across the periodic table, predicting that TcS_2 and ReS_2 are the most stable. The pyrite-type compounds seem to increase in stability as one goes across and down the periodic table. Thus, OsS_2 is the most stable pyritic compound using this test of stability. Since the trends in stability are opposite for the two tests, both stability criteria must be

considered when choosing a catalyst. From this analysis, the compounds with intermediate values of Gibbs free energy, for example layer compounds MoS_2 and WS_2 and pyritic RuS_2, should promise to be the most stable under catalytic conditions.

TABLE 2

Most stable oxide form of the transition metals.[4]

VB	VIB	VIIB	VIII
---	---	Mn_3O_4	$Fe_3O_4(Fe_2O_3)$
Nb_2O_5	MoO_3	Tc_2O_7	RuO_2
Ta_2O_5	WO_3	Re_2O_7	OsO_4

TABLE 3

Calculated Gibbs Free Energy (kcal/mole) for Reaction 4 at 298K and 1 atm pressure.[1-3]

VB	VIB	VIIB	VIII
---	---	MnS_2(14.1)	FeS_2(19.800)
NbS_2(-7.55)	MoS_2(52.389)	TcS_2(115.85)	RuS_2(79.635)
TaS_2(-24.85)	WS_2(25.528)	ReS_2(87.2595)	OsS_2(163.194)

The thermodynamic calculations given above predict that besides MoS_2, RuS_2 should be one of the more stable catalysts. As described previously, RuS_2 possesses a very different structure than that of MoS_2. Catalytic ability may be enhanced by a pyritic structure due to the probability that all of the exposed surface may be active. With the layered MoS_2, only the edge planes are active whereas the basal plane is relatively inactive.

Experimental

The RuS_2 catalysts were prepared by the method of Pecoraro and Chianelli.[5] This method was modified so that α-$RuCl_3$ could be used instead of $RuCl_4$. Lithium sulfide, Li_2S, was used as the sulfide source. Two different solvents were used, ethyl acetate and methanol. The α-$RuCl_3$ was obtained from ALDRICH and from STREM. All other chemicals were obtained from ALDRICH. The preparations were performed in an N_2-filled glove box that was vented a the hood. The N_2 was needed due to the pyrophoric nature of the amorphous RuS_2. The general procedure involved mixing the α-$RuCl_3$ with ≈300 ml of the solvent. An appropriate amount of Li_2S was dissolved in a separate 100 ml quantity of solvent to form a yellow solution. The Li_2S solution was then added to the α-$RuCl_3$ slurry while stirring. The reaction was allowed to stir for ≈16 hr. At the end of 16 hr , the stirrer was turned off and the precipitate was allowed to settle. Decantation of the solvent and washing of the precipate was followed by filtering in a Buchner funnel. Portions of a 12% acetic acid/ethyl acetate solution were used to wash the precipitate while in the funnel. The precipitate was then dried by suction of N_2 through the Buchner funnel.

Pretreatment of the amorphous precipitate was carried out at 500°C (1-2 hr) using 14.8% H_2S/H_2 at a flow rate of ≈60 cc/min. Approximately 1-2 g of the amorphous precipitate was dispersed over pyrex beads and loaded into a quartz tube under N_2. Stopcocks were attached to the ends of the quartz tube to prevent air exposure. The quartz tube was attached to the 14.8% H_2S/H_2 lines, which had been flushed prior to the attachment to avoid air exposure of the catalyst. The required flow rate of the H_2S/H_2 mixture was set, and this flow maintained over the catalyst at room temperature for 15-30 min. The temperature was then raised to just above the boiling point of

the solvent (BP(CH_3OH) = 65°C, BP(ethyl acetate) = 76.5-77.3°C, BP(acetic acid) = 116-118°C) for 30 min. The temperature was then raised to 500°C and kept at this temperature for 1-2 hr. The heat was turned off and the tube allowed to cool under flowing H_2S/H_2. Unloading of the tube occurred in the glove box under N_2.

The X-ray diffraction patterns for the samples were obtained using a Phillips Diffractometer consisting of a XRG 3100 X-Ray generator coupled with an APO 3600 control unit. Cu K_α radiation of wavelength 1.54060 Å was used to irradiate the sample, and scans were conducted using a step size of 0.02° and scan rate of 1.0°/min. The XRD was used for peak identification and determination of the particle size using the Scherrer equation.

X-ray photoelectron spectroscopy was conducted using a high resolution SCIENTA ESCA-300 instrument equipped with a monochromatic Al K_α rotating anode. The general parameters used for survey scans were pass energy, 300 EV; step size, 0.5 eV; and slit width, 1.1 mm. The general parameters used for regional scans were pass energy, 75 eV; step size, 0.05 eV; and slit width, 1.1 mm. The pressure in the sample chamber remained in the low 10^{-9} to high 10^{-10} (mbar) range. The samples studied were loaded into the ESCA using N_2-filled glove bag to avoid air exposure.

Angle resolved ESCA of a MoS_2 single crystal was carried out with the SCIENTA ESCA-300 instrument. The single crystal was cleaved under N_2 to expose a fresh surface plane. This sample was loaded onto a sample holder such that the MoS_2, when placed into the instrument, was positioned at the epicenter of the polar angle rotational axis (tilt axis). This ensured that the MoS_2 was tilted around a single line and did not swing upon polar angle incrementation. Parameters used to obtain the spectra were a pass energy of 75 eV, 1.1 mm slit width, swept mode, and with spatial lens. The general

procedure involved choosing an azimuthal angle and designating it to be some arbitrary angle. The sample at this position was subsequently noted. The Mo 3d, S 2s and S 2p spectra were obtained at this azimuthal angle for different polar angles. The polar angle was increased in 2° increments from -20°(340°) to +70°. At a polar angle of 0°, the sample surface was perpendicular to the detector. At polar angles of ≈56°, the cap that was placed on top of the sample to hold it in place, begins to interfere with the intensities of the collected peaks. Prior to azimuthal angle incrementation, the spectra for a polar angle of -20° was duplicated to check the reproducibility of the instrument. The azimuthal angle was then incremented by 10° and the whole procedure was repeated at this azimuth. In all, spectra for 10 azimuthal angles were collected, resulting in 450 data files. The area under the peaks could be found from a curve fitting routine and plotted vs. polar angle or azimuthal angle. The first angle resolved ESCA study discussed previously employed the monochromatic Al K_α rotating anode of energy 1486.6 eV.[6] The second study employed the nonmonochromatized Mg K_α conventional anode of energy 1253.6 eV. A Laue diffraction pattern of the MoS_2 single crystal used in these studies will be used to gain knowledge about the orientation of the crystal surface.

Five-point BET surface areas were obtained using a Digisorb 2500 instrument. Helium was used to calibrate the dead volume and the adsorbate was N_2. Elemental analyses were carried out by Gailbraith Laboratories. Samples were weighed under N_2 prior to any exposure.

Results and Discussion

The RuS_2 catalyst was initially prepared by the method of Pecoraro and Chianelli.[5] This method employed α-$RuCl_2$, Li_2S, ethyl acetate solvent, and a 12% acetic acid wash. The acetic acid wash was used to remove all of the LiCl product impurities. Some problems were encountered with this preparation. One problem consisted of the insolubility of the $RuCl_3$ in the ethyl acetate. A second problem was that the acetic acid wash did not remove all of the LiCl impurities and could not remove any other contaminants. Other contaminants would include unreacted α-$RuCl_3$ and Li_2S. The amorphous form of this catalyst was designated RUS2-300, while the crystalline, pretreated form was designated RUS2-310. Elemental analyses of these catalysts are shown in Table 4. The RUS2-310 was pretreated for 1 hr at 500°C. The sulfur ruthenium mole ratios are very low in these two catalysts probably due to the presence of unreacted $RuCl_3$ and Ru(0).

TABLE 4

Results of elemental analyses of different RuS_2 preparations. The values in the table are weight percentages. The S/Ru ratio is a mole ratio calculated from the weight percentages.

Element	Theoretical	RUS2-300	RUS2-310	RUS2-340	RUS2-520	RUS2-610
%Ru	61.18	38.83	53.24	61.33	57.65	56.81
%S	38.82	22.29	29.71	33.30	38.29	37.98
%Li	---	0.947	1.29*	0.055	0.95	1.32
%Cl	---	8.33	11.4*	<0.16	1.81	1.49
Total%	100	70.397	95.64	94.845	98.70	97.60
S/Ru	2.000	1.809	1.760	1.710	2.094	2.11

*These values were calculated from the ruthenium/lithium, chlorine mole ratio of the RUS2-300.

A cleanup of the products of the preceding preparation was attempted using methanol. Methanol was chosen because α-$CuCl_3$ is sparingly soluble, Li_2S is soluble, LiCl is soluble to 42.36 g/100 cc, and RuS_2 is insoluble in this solvent. The procedure was to add the precipitate to ≈300 ml of CH_3OH and stir for 2 hr. The precipitate was allowed to settle, the CH_3OH was decanted, and ≈300 ml CH_3OH again added. This time the solution was stirred for 16 hr. The precipitate was allowed to settle prior to the second decantation of the CH_3OH. In the next step, the precipitate was filtered and washed with two portions of ≈35 ml solvent. The precipitate was allowed to dry under N_2. A small portion of this sample was pretreated for 1 hr and designated RUS2-340. The elemental analysis of this sample is shown in Table 4. The CH_3OH cleanup removed a majority of the Li and Cl impurities. However, the mole ratio of S/Ru = 1.71 indicates an excess of ruthenium. XRD and ESCA analyses of this sample were carried out to probe the nature of the excess ruthenium.

The XRD pattern of the RUS2-340 is shown in Figure 1. Peaks could be assigned to Ru(0) and RuS_2 as noted in the pattern. The excess ruthenium is present in the bulk as ruthenium metal. However, this sample was pretreated with 14.8% H_2S/H_2 and the surface may have a very different character than that of the bulk. ESCA was used to study the surface and will be discussed in the following paragraphs. Particle sizes, t, of the RuS_2 and Ru(0) can be calculated from the XRD patterns using the Scherrer equation (5).[7] A preliminary particle size can be obtained if the full width at half maximum, FWHM, of a highly crystalline sample, w', is considered to be much smaller than the FWHM of the peaks under consideration. The FWHM of the peak is physically measured from an enlarged version of the XRD pattern. The average particle sizes calculated for the RuS_2 and Ru(0) are given in Table

5. A surface area can be calculated from the particle size assuming that the particles are approximately spherical. The density of the RuS_2 can be calculated from the lattice cell dimensions and the number of molecules of RuS_2 per unit cell as shown in Equation 6. An estimated RuS_2 surface area, Equation 7, can be calculated from the density and particle size assuming spherical particles. The particle size is the diameter of the spherical particle.

$$t = \frac{0.89\lambda}{(W_x^2 - w'^2)^{1/2}\cos\theta} \qquad (5)$$

t = diameter of the particle in Å
λ = wavelength of radiation (1.54060 Å)
W_x = FWHM of peak in radians
w' = FWHM of highly crystalline sample (instrumental FWHM)
θ = Bragg angle of diffraction (1/2 angle between diffracted and transmitted beam)

$$\frac{1 \text{ unit cell}}{(5.6096\ \text{Å})^3} \times \frac{4 \text{ molecules } RuS_2}{\text{unit cell}} \times \frac{1}{N_A} \times \frac{165.19 \text{ g } RuS_2}{\text{mole } RuS_2} = 6.22\times10^{-24} \text{ g } RuS_2/\text{Å}^3 \qquad (6)$$

$$\frac{\text{Area (sphere)}}{\text{Volume(sphere)}} \times \frac{1}{p} \rightarrow \frac{4\pi r^2}{4/3\pi r^3} \times \frac{1}{p} \rightarrow \frac{3}{rp} \rightarrow \frac{6}{tp} \qquad (7)$$

TABLE 5

Particle sizes (t) and surface areas (SA) of the RuS_2 samples listed.

Sample	$\langle t\rangle RuS_2$ (Å)	$\langle t\rangle Ru$ (Å)	Estimated RuS_2 SA (m^2/g m)	RuS_2 BET SA (m^2/g)
RUS2-340	170	130	57	---
RUS2-520	180	---	54	---
RUS2-610	230	---	42	7.0

A third preparation using CH_3OH as the solvent was attempted. The α-$RuCl_3$ starting material was mixed with ≈300 ml of solvent. An appropriate amount of Li_2S was dissolved in ≈100 ml of solvent to form a yellow solution. This Li_2S solution was added, while stirring to the $RuCl_3$ slurry. The reaction was allowed to proceed for 16 hr. The precipitate was allowed to settle before decantation of the solvent. Successive washings followed by filtering and drying under N_2 followed. The 1 hr pretreatment proceeded as before and the crystalline RuS_2 obtained was designated RUS2-520. The elemental analysis of this compound is shown in Table 4. Very stoichiometric RuS_2 was obtained by this procedure as seen by the S/Ru mole ratio. However, significant amounts of Li and Cl remain. The XRD of the RUS2-520 indicates only the presence of crystalline RuS_2, and particle sizes and estimated surface areas were calculated as shown in Table 5.

A larger scale RuS_2 preparation (designated RUS2-610) was also performed using CH_3OH as the solvent. The same procedure was used as in the preceding paragraph, but, the pretreatment was extended to 2 hr. Elemental analysis, as seen in Table 4, showed a much higher S/Ru mole ratio of 2.11. Impurities of Li and Cl still remained at significant levels. The XRD pattern shown in Figure 2 indicates only the presence of RuS_2, and that no bulk Ru(0) existed in the catalyst. The surface area was measured by a 5-point BET and also calculated from the XRD pattern (shown in Table 5). The large discrepancy between the experimental and the calculated surface areas might be due to error inherent in the Scherrer equation.

The impurity levels seem to depend on the dryness of the solvent. During the last preparation, the Li_2S initially formed a yellow solution when mixed with the CH_3OH solvent. After a few minutes, a white precipitate formed that was insoluble in the CH_3OH. Although the precipitate has not

been tested, its presence can be attributed to H_2O contaminating the CH_3OH. The Li_2S will react with H_2O to form LiOH and H_2S, and standard references indicate that LiOH is sparingly soluble in alcohols. The presence of high levels of Li in the products can be attributed to formation of LiOH. The presence of Cl can be attributed to incomplete reaction of $RuCl_3$. Future RuS_2 preparations will rigidly exclude the presence of H_2O in the solvent.

Although Pecoraro and Chianelli discuss their preparation, e.g. Equation 8, in detail, a chemical equation for a starting material of α-$RuCl_3$ is not as simple. A chemical equation sequence (Equations 9a and 9b) can be proposed that accounts for the formation of Ru(0) particles in some of the preparations. If the sulfidization is not complete, Ru(0) will be seen in the XRD pattern, e.g. as seen in the sample RUS2-340. The longer sulfidization (2 hr pretreatment) of the RUS2-610 effectively eliminated the bulk Ru(0).

$$RuCl_4(s) + 2\ Li_2S(s) \rightarrow RuS_2(s) + 4\ LiCl(s) \qquad (8)$$

$$4\ RuCl_3(s) + 6\ Li_2S(s) \rightarrow 3\ RuS_2(s) + Ru(s) + 12\ LiCl(s) \qquad (9a)$$

$$Ru(s) + 2\ H_2S(g) \rightarrow RuS_2(s) + s\ H_2(g) \qquad (9b)$$

A preliminary high pressure reactor study was carried out with the RUS2-310 catalyst. This catalyst had a bulk S/Ru mole ratio of 1.760, and the conditions used were outlined in the experimental section. During the entire testing procedure the total flow fluctuated by not more than 4%. After pressurization, the temperature of the catalyst bed was increased to 250°C. No significant activity was seen at reactor temperatures between 250°C-300°C. At temperatures above 300°C (up to a maximum temperature of

320°C), trace amounts of lower hydrocarbons and CO_2 were produced.

HR-ESCA Analyses of the Catalysts. Valence band spectra have also been obtained for polycrystalline RuS_2, MoS_2 and NbS_2 by high resolution ESCA. The experimental valence bands can be compared to the theoretical valence bands available in the literature. In an attempt to attain better valence band spectra, the phenomena of charging was investigated for the RuS_2 sample. The nature of the ESCA experiment causes a depletion of the electrons on the surface of the sample. Due to a partial positive charge on the surface, electrons will be held tighter by the surface atoms causing a corresponding increase in the binding energy. This causes a broadening and shifting of the photoelectron peaks to higher binding energies. Metallic conductors will not charge since electrons are available in the conduction band to replace the electrons lost in the ESCA experiment. Insulators, on the other hand, do not have electrons in the conduction band available to replace the lost electrons and charging results. A flood gun can be used to partially neutralize this positive charge by flooding the surface of the sample with electrons.

RuS_2 is a small band gap semiconductor and could be expected to have a small amount of charging. The flood gun was used to try to neutralize any charging. The RuS_2 proved to be insensitive to the flood gun and thus charging does not seem to be a problem with this sample. The experimental valence band of RuS_2 is shown in Figure 3, of MoS_2 in Figure 4 and of $NbS_{1.75}$ in Figure 5. The semiconductor nature of the RuS_2 and MoS_2 can be seen in the indicated spectra since the electron density falls to zero before a binding energy of 0 eV is reached. The conduction level is unfilled at room temperature. However, the $NbS_{1.75}$ valence band spectra shows the characteristic shape of a metallic Fermi edge of finite width at

the zero of binding energy. Thus, an occupation of the conduction levels at room temperature is indicated. The intense peak right below the fermi level in RuS_2 is attributed to the crystal field split triply degenerate 4d t_{2g} level of the ruthenium. This level is fully occupied by six electrons/Ru^{+2}. The remaining peaks at higher binding energies are attributed to the S 3p bands.

The MoS_2 valence band spectra also exhibits this characteristic 4d level split by the crystal field. This time the level is a nondegenerate d_z^2 band occupied by two electrons/Mo^{+4}. The lower intensity of the Mo d_z^2 when compared to that of the Ru t_{2g} band to a first approximation can be caused by the different number of electrons in this band. The RuS_2 contains S_2^{2-} (10 S 3p valence electrons) species and the MoS_2 contains 2 S^{2-} (12 S 3p valence electrons) species. An approximate comparison of the valence bands can be obtained from a comparison of the ratio Area Metal 4d/Area S 3p. The experimental Ru 4d/S 3p ratio is 0.9819, the ratio for MoS_2 is 0.3121 and the ratio for the $NbS_{1.75}$ is 0.1701. If the differences in these ratios are attributed to the number of electrons in the M 4d and S 3p levels then the ratio for RuS_2/MoS_2 should be close to the theoretical ratio of (6/10)/(2/12) or 3.6. The experimental ratio (Ru 4d/S 3p)/(Mo 4d/S 3p) = 3.146, which is very close to the predicted ratio of 3.6. The ratios of MoS_2/NbS_2 and RuS_2/NbS_2 can also be calculated and are shown in Table 6. The experimental ratio for the Ru/Nb is very low, and one reason for this low value could be due to the extra niobium atoms in $NiS_{1.75}$. The extra niobium atoms are probably intercalated in between the layers and contribute electrons to the conduction band of the sulfide. This contribution will lower the experimental ratio by making the Nb 4d area larger.

TABLE 6

Theoretical Electron Ratios Compared to Experimental Area Ratios.

Ratio	Theoretical Electron Ratio	Experimental Area Ratio
$\frac{\text{Ru 4d/S 3p}}{\text{Mo 4d/S 3p}}$	3.6	3.146
$\frac{\text{Mo 4d/S 3p}}{\text{Nb 4d/S 3p}}$	2.0	1.835
$\frac{\text{Ru 4d/S 3p}}{\text{Nb 4d/S 3p}}$	7.2	5.772

A curve fitting procedure was used to examine the valence band of RuS_2 in greater detail. The Ru 4d t_{2g} peak was fit to a Gaussian centered at a binding energy of 1.67 eV. A FWHM of 1.40 eV was obtained. The peaks from ≈3-10 eV are due to the S 3p electrons, and those centered around 15 eV are attributed to the S 3s electrons. This spectra can be compared to the present theoretical density of states as calculated by Holzwarth et al.[8] The experimental spectra compares favorably with the theoretical density of states.

The MoS_2 valence band, Figure 4, can also be fit to Gaussians using the same curve fitting routine. A FWHM for the d_{z^2} band of 1.23 eV is obtained. This value compares very well with the theoretical d_{z^2} level of 1.3 eV found by Bullett.[9] Qualitatively, the experimental valence band spectra compares well with the theoretical results. Some important features are that the d_{z^2} level overlaps the wide S 3p bands to a finite extent and the S 3s bands are widely separated from the S 3p.

The $NbS_{1.75}$ valence band spectra shown in Figure 5 can be discussed in terms of stoichiometric NbS_2. Extra Nb atoms may be present in between the layers of this sample. As mentioned previously, the extra Nb atoms can cause electron donation to the d_{z^2} band. Since the MoS_2 and NbS_2 compounds

have approximately the same structure, the valence band can be compared. Again, a wide S 3p region is obtained that is widely separated from the S 3s region. However, there are some finite differences in the two S 3p band regions. These differences may be due to the lack of stoichiometric NbS_2 and/or due to the different stacking in the c direction. This phenomena needs further investigation prior to reaching a definite conclusion. The valence band regions of RuS_2, MoS_2 and NbS_2 are being investigated by use of the computer program EHMACC. The program is used to calculate the energies and Bloch functions for specific high symmetry points in the lattice. The end result is a calculated density of states that can be compared to the experimental valence band regions obtained by ESCA. The experimental d_{z^2} band of the $NbS_{1.75}$ has a FWHM of 1.12 eV. The value is comparable to the theoretical band width obtained by Bullett for $NbSe_2$ (1.1 eV).[9] The metallic character of the $NbS_{1.75}$ can be seen at the binding energy of 0 eV. A Fermi edge width, Figure 6, can be calculated by finding the difference in binding energies at 88% maximum height of the edge and at 12% maximum height. From this type of calculation, a Fermi edge width of 0.66 eV is obtained. The instrumental Fermi edge width is 0.33 eV under the conditions used for this experiment.

The angle resolved ESCA studies of the MoS_2 single crystal are still in the preliminary stages of investigation. More thought must be given to the properties of the emitted photoelectron. Can the photoelectron be truly represented by a spherical wave (like an electron in an s orbital) or do the actual quantum mechanics of the situation dictate that the change in angular momentum, Δl, be ± 1? If the Mo 3d electron is incremented by -1, a p-type orbital results. The inclusion of this section rule into the theory could change the interpretation of the previous experiments in the literature. A

solution to the debate of forward focusing vs. shadowing of the photoelectrons is sought. Theoretical calculations predicting the angular behavior of photoelectrons emitted from MoS_2 in the forward focusing regime must be attempted. The theoretically predicted angle resolved pattern can then be compared to the experimental study.

A preliminary prediction as to where forward focusing of the Mo 3d electrons will occur can be made. Figure 7, displays the geometry of the basal plane of MoS_2. This surface of this plane is known to contain exposed and unsaturated sulfur ligands. The Mo (referred to here as the second atomic layer) lies below the exposed sulfur ligands (referred to as the first atomic layer). A photoelectron from the Mo 3d level of the second atomic layer can be forward focused (according to the theory) by the sulfur ligands that lie above it. The angle between the perpendicular to the basal plane and Mo-S bond is 49.1°. Forward focusing of the second layer Mo 3d electrons should occur at a polar angle of 49.1° for three different azimuthal directions (which are 120° apart). A graph of the Mo $3d_{5/2}$, S 2p and S 2s areas vs. polar angle for an arbitrary azimuthal angle of 10° is shown in Figure 8. Maxima occur for polar angles: -18, 0, 16, 34 and 54. A similar graph for an azimuthal angle of 50° is shown in Figure 9. Maxima occur at somewhat different polar angles: -14, 0, 30, 50. A peak occurring at 49.1° is predicted from forward focusing arguments. The intense peak at a polar angle of 50° appears in the plot for azimuthal angle of 50° and not for that of 10°. A different way to plot the data was used to examine this feature. The area Mo $3d_{5/2}$ vs. azimuthal angle, Figure 10, was plotted for polar angles of 0°, and 48°. For a polar angle of 0° the line connecting the points shows small deviations with azimuthal angle. Marked deviations in the Mo $3d_{5/2}$ area with azimuthal angle are seen. The Mo $3d_{5/2}$ area

is largest at an azimuthal angle of 50°. If more spectra had been obtained at different azimuthal angles, two more intense peaks at azimuthal angles of 170° and 290° should have been seen as predicted.

The above discussion centered on the data obtained using the monochromatic Al K_α rotating anode. An angle resolved study was also carried out using the Mg K_α conventional anode. This study was done in an attempt to separate any diffraction peaks (in the plots of area vs. polar angle) from forward focused peaks. Using Bragg's Law, which assumes that the electrons are plane waves instead of spherical waves, an estimate of the polar angle diffraction maxima can be obtained for the different wavelength of radiation used. The ratio of wavelengths, $\lambda_{Mg}/\lambda_{Al}$, is inversely proportional to the ratio of their energies, E_{Al}/E_{Mg}, which is 1.1859. A ratio of Bragg's for the two different types of radiation (Equation 10) can

$$1.1859\sin\theta_{Al} = \sin\theta_{Mg} \qquad (10)$$

be used to predict the polar angle of diffraction of Mg K_α radiation, θ_{Mg}, from θ_{Al}. Diffraction peaks of 16°, 32° and 48° obtained using Al K_α radiation will be shifted to corresponding polar angles of 19°, 39° and 62° when Mg K_α radiation is used. This research is still in the preliminary stages of examination. More tests need to be done before accurate conclusions can be drawn from the experimental data. Further tests include Laue diffraction of the single crystal used in the study of angle resolve ESCA of polycrystalline MoS_2. The Laue diffraction will lead to information about the orientation of the crystal and direction of the Mo-S bond. Angle resolved ESCA of polycrystalline MoS_2 can be obtained for polar angles in only one azimuthal direction. This last study will rule out the assumption that geometrical factors cause the observed variations in polar angle.

B. Niobium Disulfide Catalysts

Analysis of Purchased Sample

The purchased sample sold as $NbS_{1.75}$ and having the stoichiometry $NbS_{1.55}$ by elemental analysis was characterized by HR-ESCA and XRD. Even though the sample was prepared and loaded under nitrogen, oxygen and carbon are present (see survey scan in Figure 11).

The valence band spectrum of $NbS_{1.75}$ (Figure 5) indicates that some electrons in the sample are in the conduction band. This is shown in the spectrum when the baseline starts in the negative binding energy region.

Since the sample was purchased from the same company that supplied the National Bureau of Standards, good agreement was obtained in the XRD pattern.[10] The major difference being that our pattern (Figure 12) shows a broad peak for the mylar film that was used to cover the sample (at 26°). All other peaks can be assigned to the niobium sulfide. This would suggest that stoichiometric NbS_2 was not obtained by NBS.

Preparation of NbS_2 Catalysts

Efforts to synthesize stoichiometric NbS_2 by precipitation were continued. The procedure to reacting $NbCl_5$ with Li_2S was improved by filtering out any LiOH formed when Li_2S is dissolved in methanol.

Possibilities of sulfiding $NbCl_5$ and Nb_2O_5 were also explored.

Preparation of NbS_2 from $NbCl_5$ and Li_2S in Methanol

This method proved successful in producing high purity RuS_2. An analogous preparation with $NbCl_5$ was tried to determine if NbS_2 would be formed.

A 2.15 g (46.8 mmol) sample of Li_2S was weighed and placed in a 200 ml beaker containing a stir bar. Stirring was commenced and 100 ml of methanol

was added. The methanol contained no more than 0.02% H_2O and had been freshly opened. A flaky white precipitate formed, probably LiOH, which could not be dissolved and was filtered out of the solution.

To a 50 ml beaker, 5.00 g (18.5 mmol) $NbCl_5$ was added and then dissolved in 50 ml methanol. This solution was added to the Li_2S-methanol solution while stirring and the solution turned black. Filtering yielded 0.4 g of a brown solid. After being pretreated for 1 hr at 500°C in 14.8% H_2S/H_2, the compound was characterized by XRD and elemental analysis. The XRD pattern did not support the presence of NbS_2 when compared to a standard pattern for NbS_2. Furthermore, elemental analysis gave a stoichiometry of $NbS_{0.51}$. Therefore, NbS_2 production by this method is not feasible.

Pretreatment of $NbCl_5$ and Nb_2O_5

$NbCl_5$ and Nb_2O_5 were pretreated in 14.8% H_2S/H_2 for 1 hr at 500°C. The $NbCl_5$ had changed color from yellow to black. The XRD pattern was not indicative of a niobium sulfide compound having a 1:2 stoichiometry. In addition, the elemental analysis revealed a stoichiometric ratio of $NbS_{0.895}$.

The Nb_2O_5 turned from white to dark gray upon pretreatment. A complex, non-typical XRD pattern was obtained. Elemental analysis showed a stoichiometry of $NbS_{0.513}$. These experiments demonstrate that unreacted starting material ($NbCl_5$) and niobium oxide, formed as a result of exposure to oxygen, cannot be recovered as from NbS_2 by pretreating with 14.8% H_2S/H_2.

REFERENCES

1. I. Barin and O. Knacke, "Thermochemical Properties of Inorganic Substances," Springer-Verlag, New York (1973).

2. I. Barin, O. Knacke, and O. Kubaschewski, "Thermochemical Properties of Inorganic Substances-Supplement," Springer-Verlag, New York (1977).

3. K. C. Mills, "Thermodynamic Data for Inorganic Sulphides, Selenides and Tellurides," Butterworths & Co., London (1974).

4. N. N. Greenwood and A. Earnshaw, "Chemistry of the Elements," Pergamon Press, New York (1984).

5. T. A. Pecoraro and R. R. Chianelli, J. Catal., 67, 430 (1981).

6. K. Klier, R. G. Herman, M. Richards, and R. D. Bastian, "Alkali/TX_2 Catalysts for CO/H_2 Conversion to C_1-C_4 Alcohols," Technical Progress Report DOE/PC/88933-6 (June 1990).

7. B. D. Cullity, "Elements of X-ray Diffraction," 2nd ed., Addison Wesley Publishing Co., Inc., Reading, Mass. (1978).

8. N. A. W. Holzwarth, S. Harris, and K. S. Liang, Phys. Rev. B, 32(6), 3745 (1985).

9. D. W. Bullett, J. Phys. C: Solid State Phys., 11, 4501 (1978).

10. Powder Diffraction, Vol. 3, No. 1 (March 1988).

Figure 1.
XRD pattern of RUS2-340.

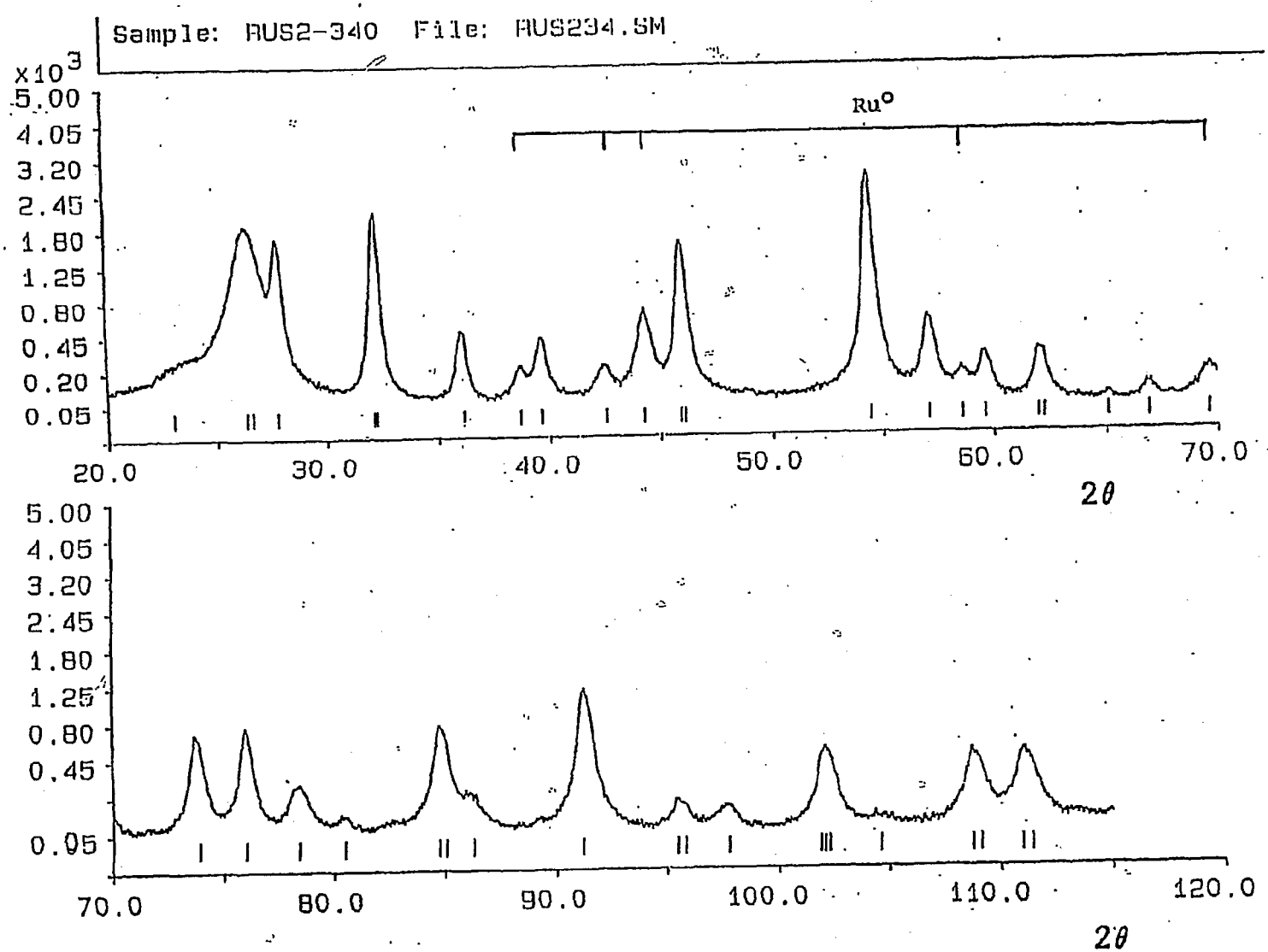

Figure 2.
XRD pattern of RUS2-610.

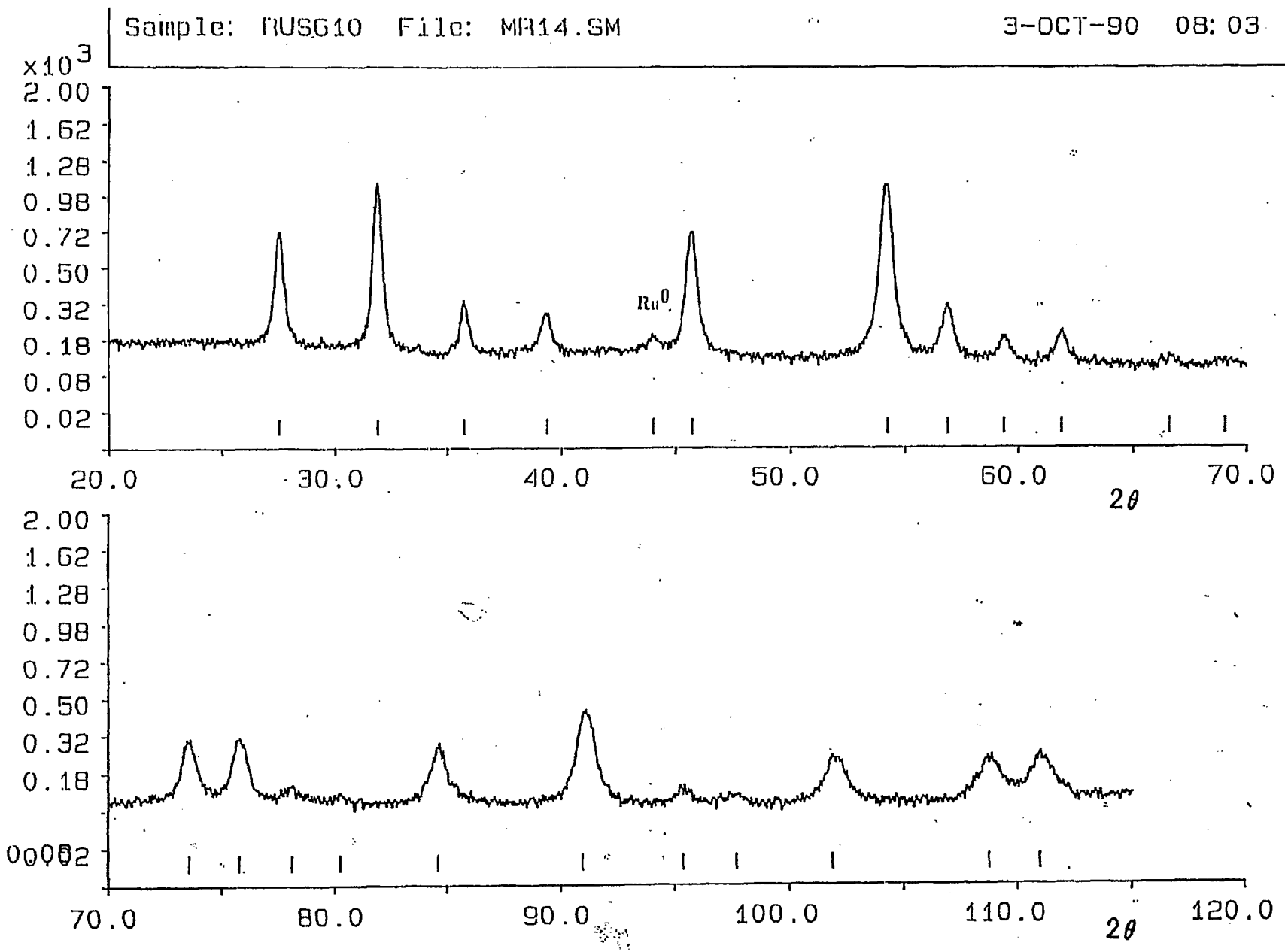

Figure 3.
Valence band region of polycrystalline RuS_2.

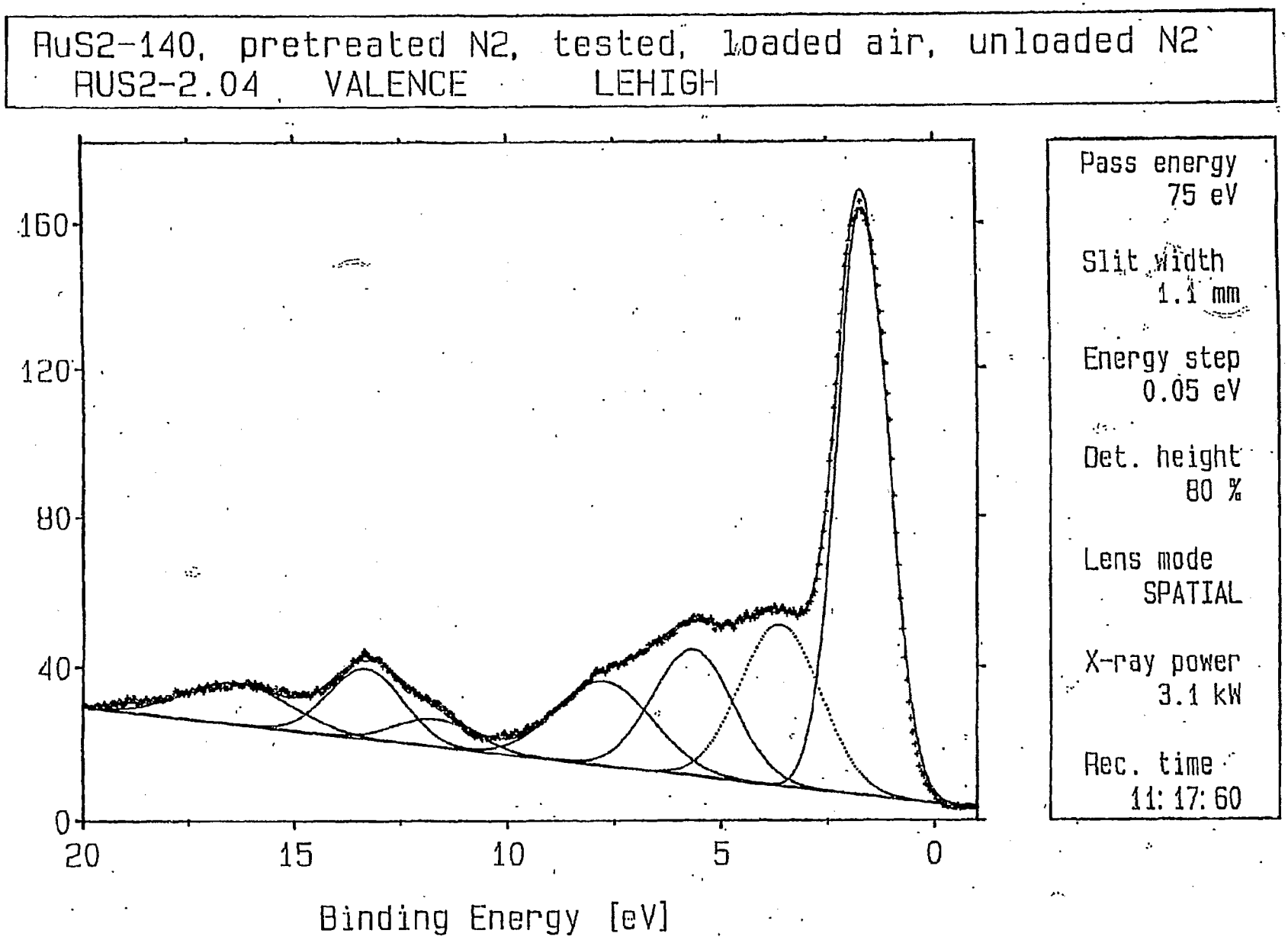

Figure 4.
Valence band region of polycrystalline MoS_2.

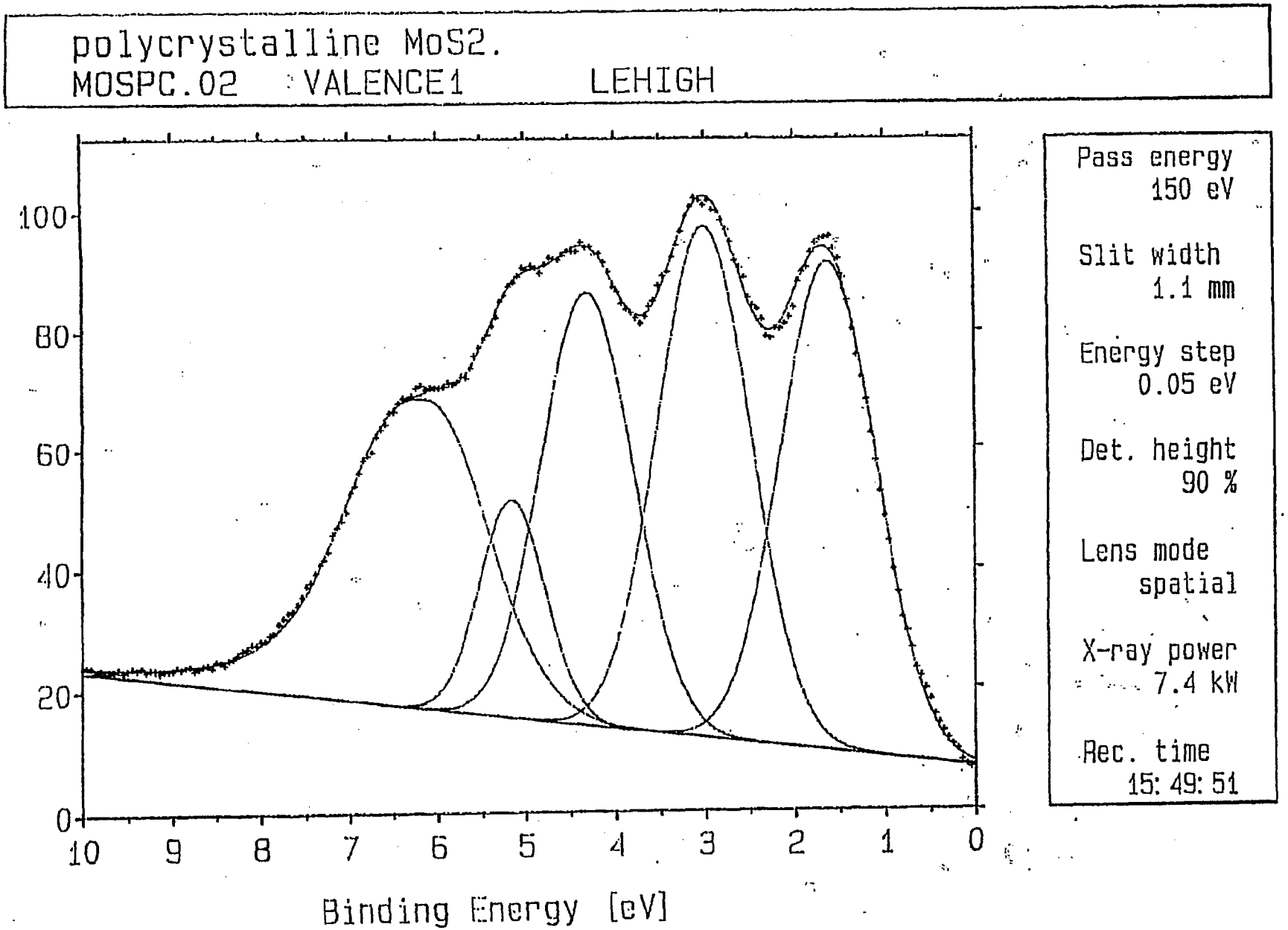

Figure 5.
Valence band region of polycrystalline $NbS_{1.75}$.

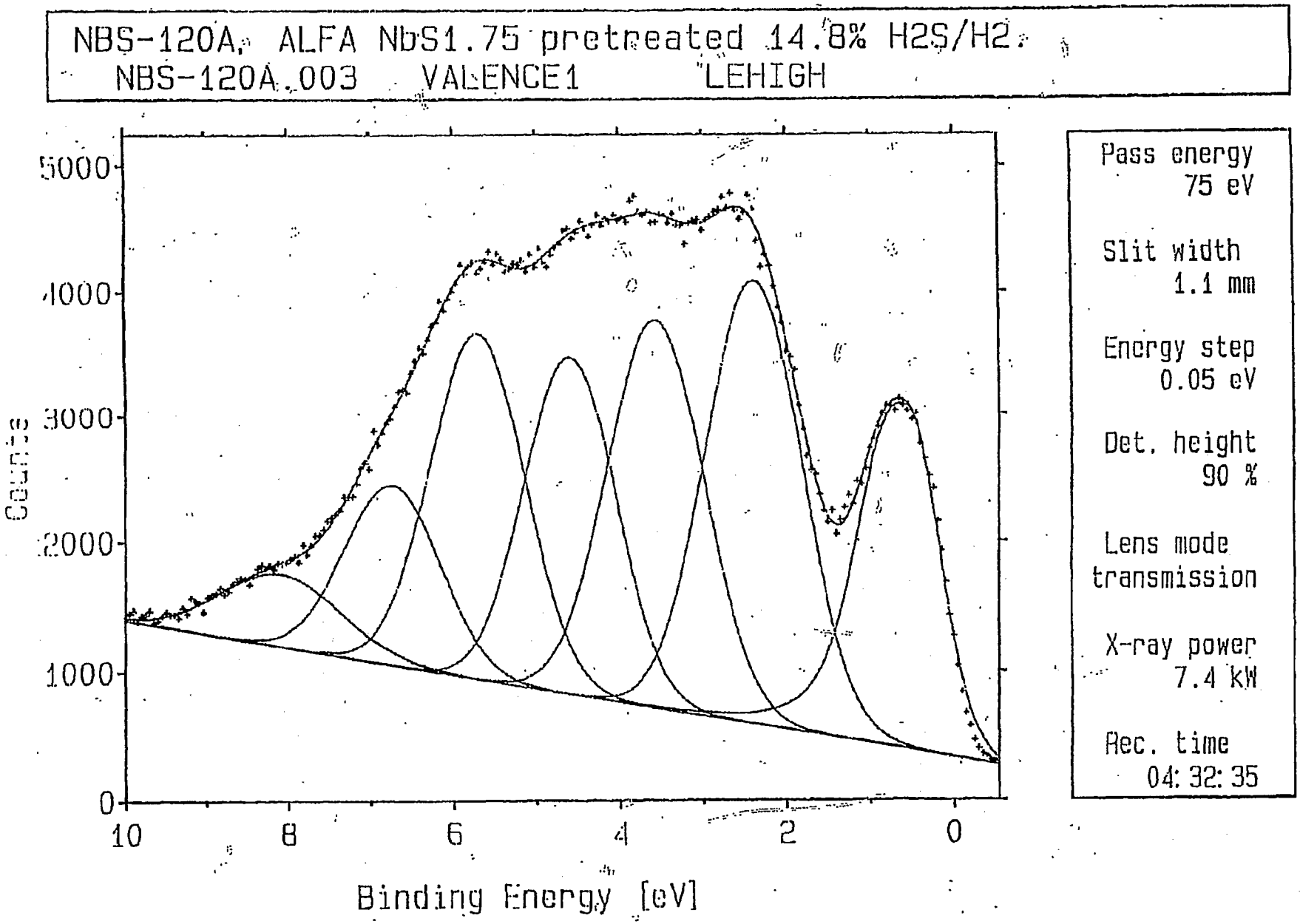

Figure 6.
Fermi edge of polycrystalline $NbS_{1.75}$.

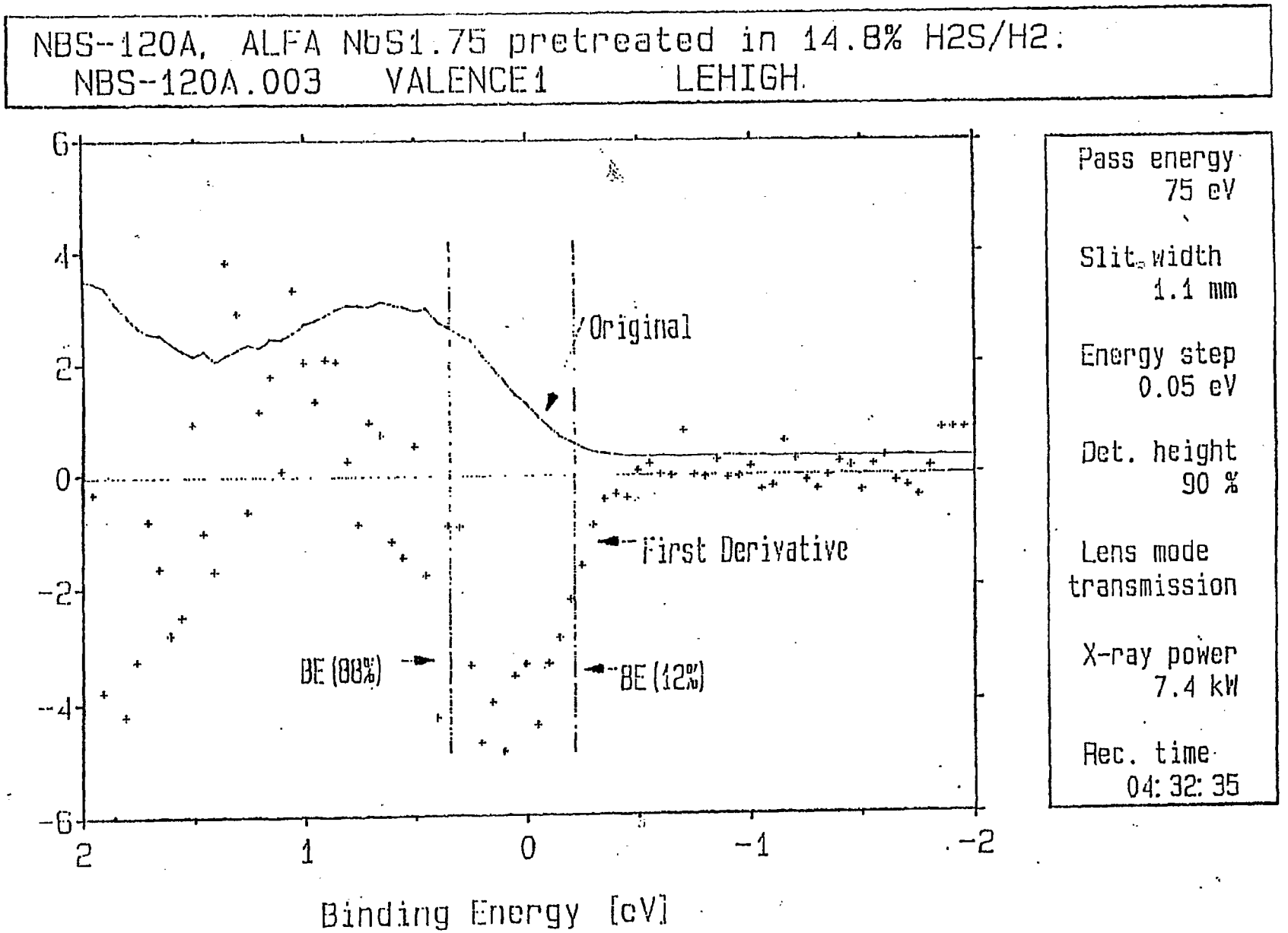

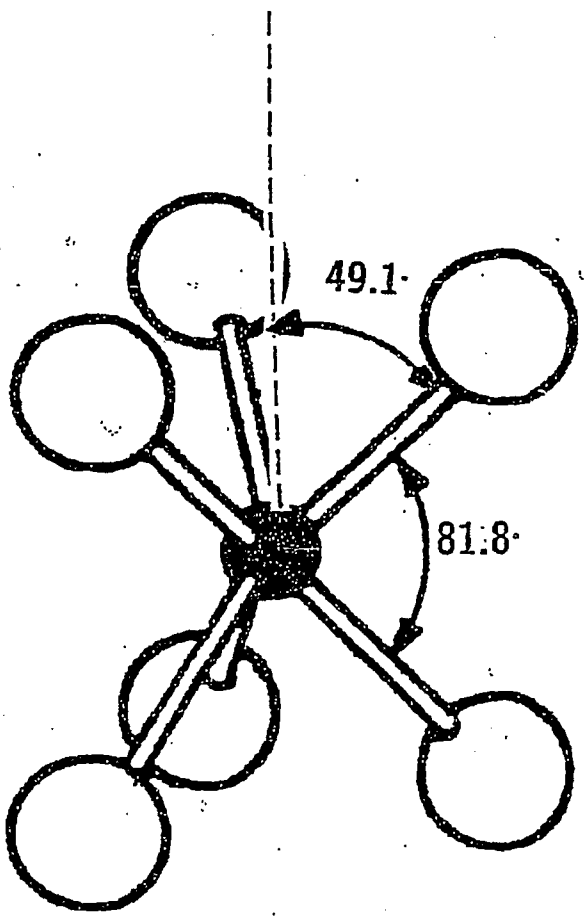

Figure 7.
Coordination of Mo by sulfur in MoS_2. A polar angle of 49.1·, as measured from the surface normal, leads to forward focusing of the Mo electrons by the sulfur ligands.

Figure 8.
Angular XPS of MoS_2 (Azimuthal angle = 10°).

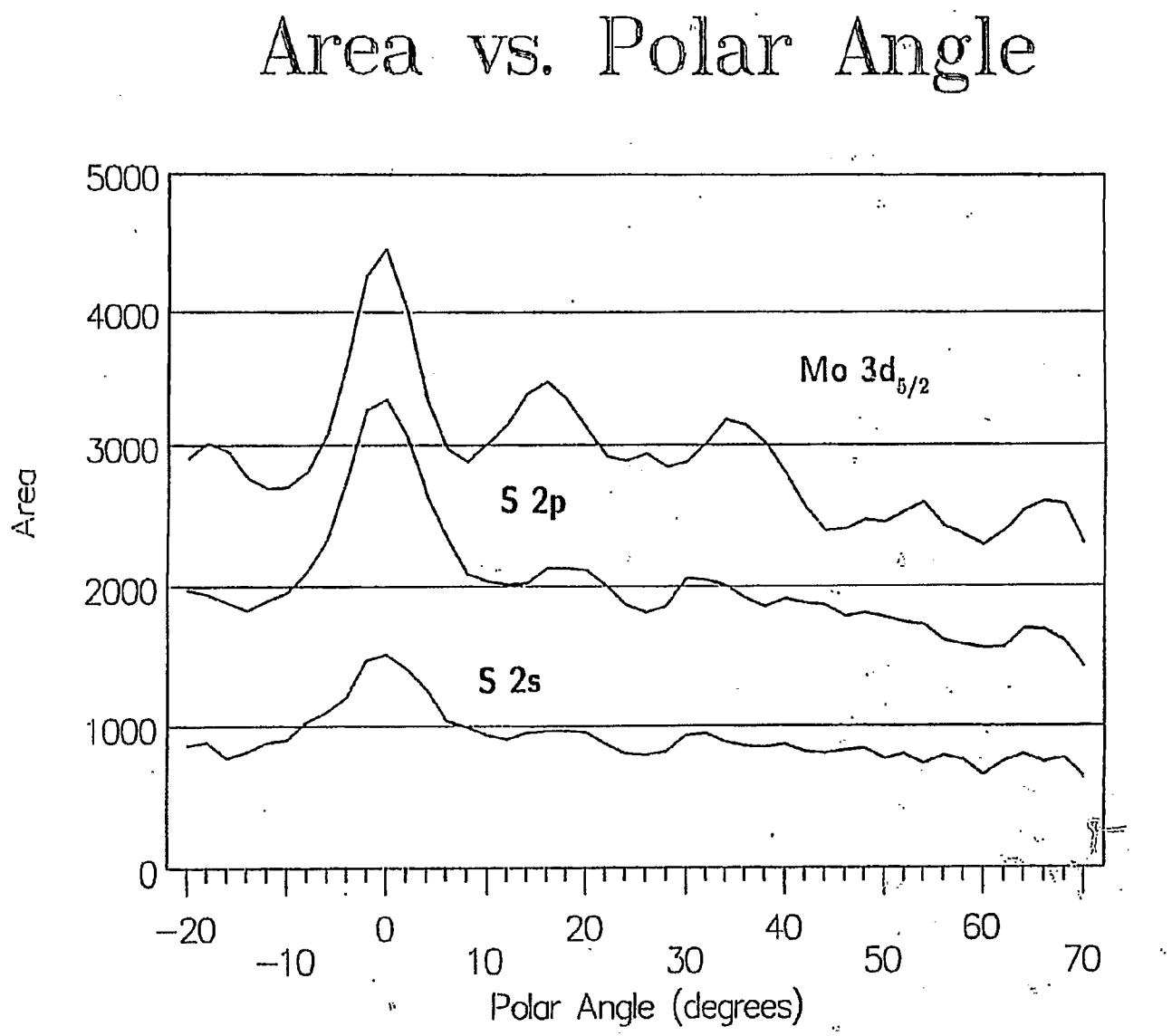

Figure 9.
Angular XPS of MoS_2 (Azimuthal angle = 50°).

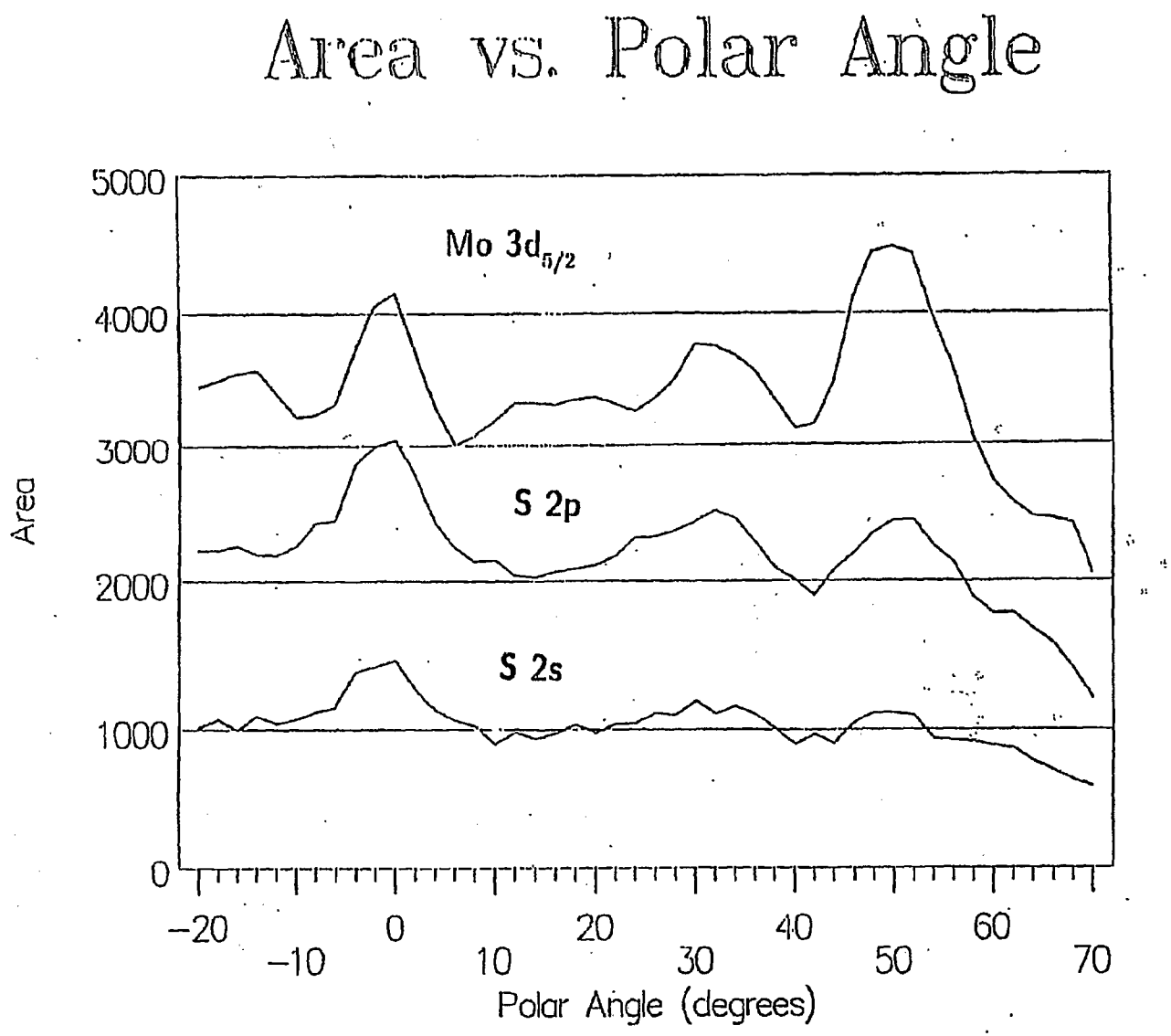

Figure 10.
Angular XPS of MoS_2.

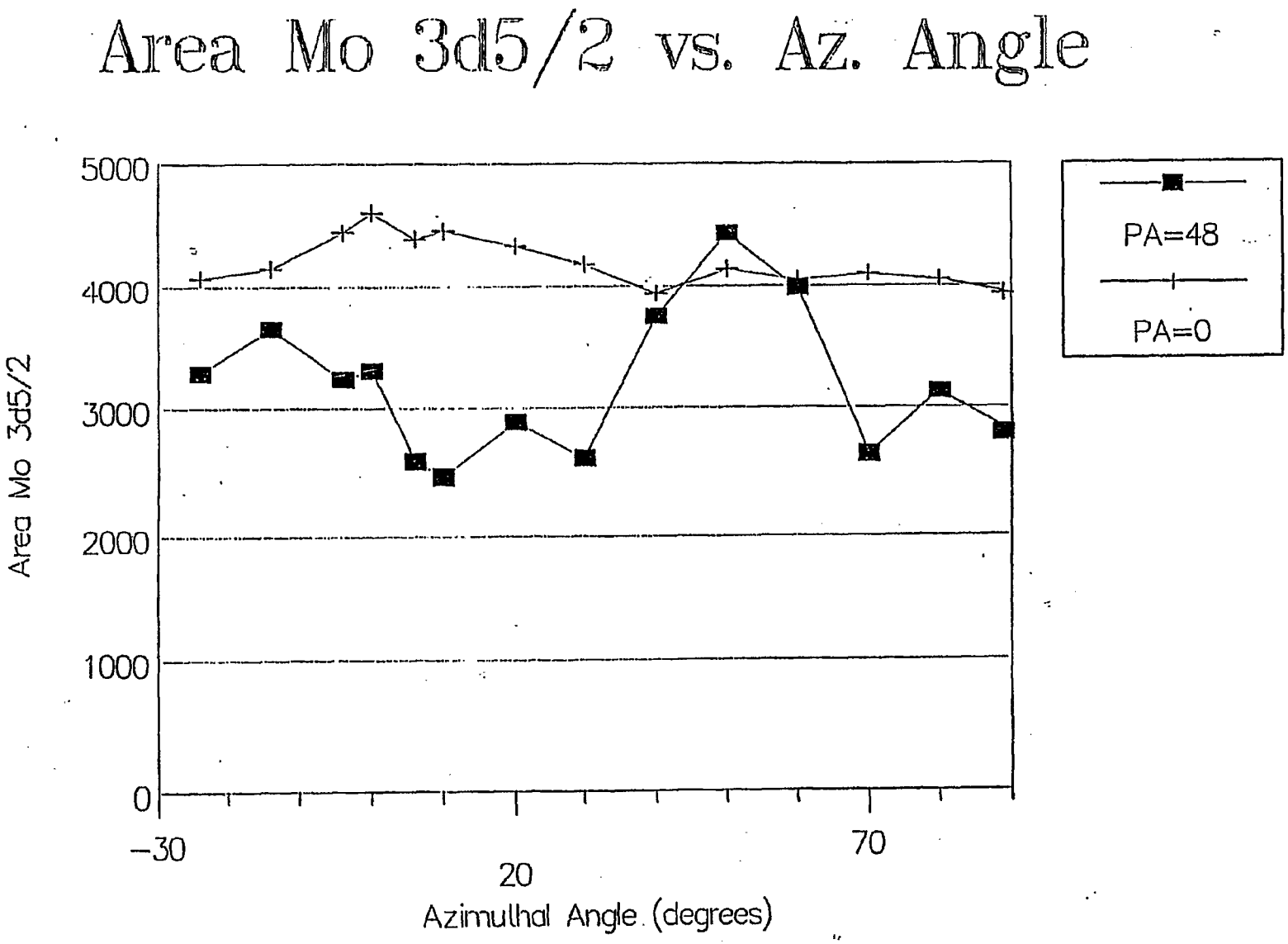

Figure 11.
HR-ESCA survey spectrum of polycrystalline $NbS_{1.75}$

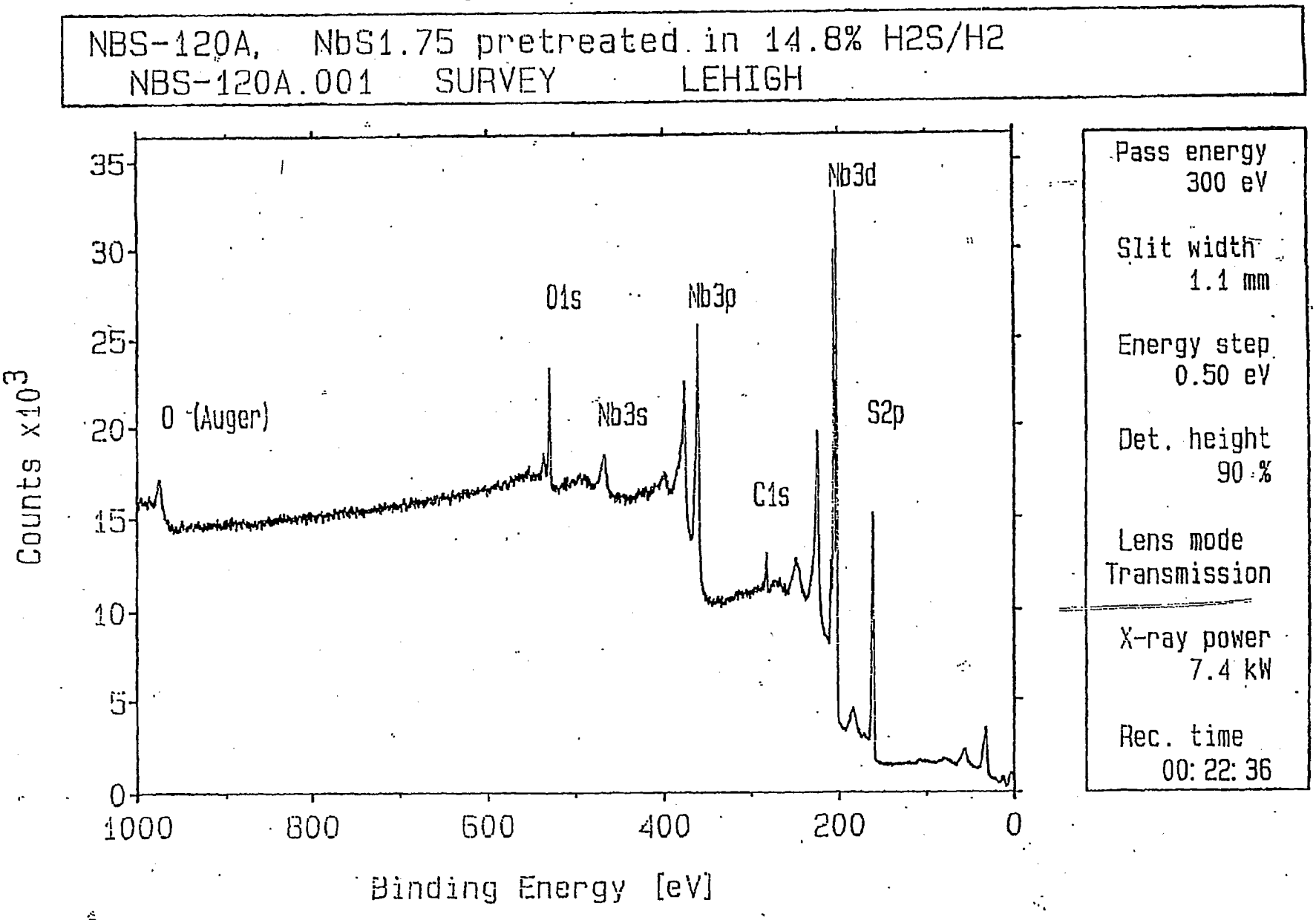

Figure 12.
XRD pattern of $NbS_{1.75}$

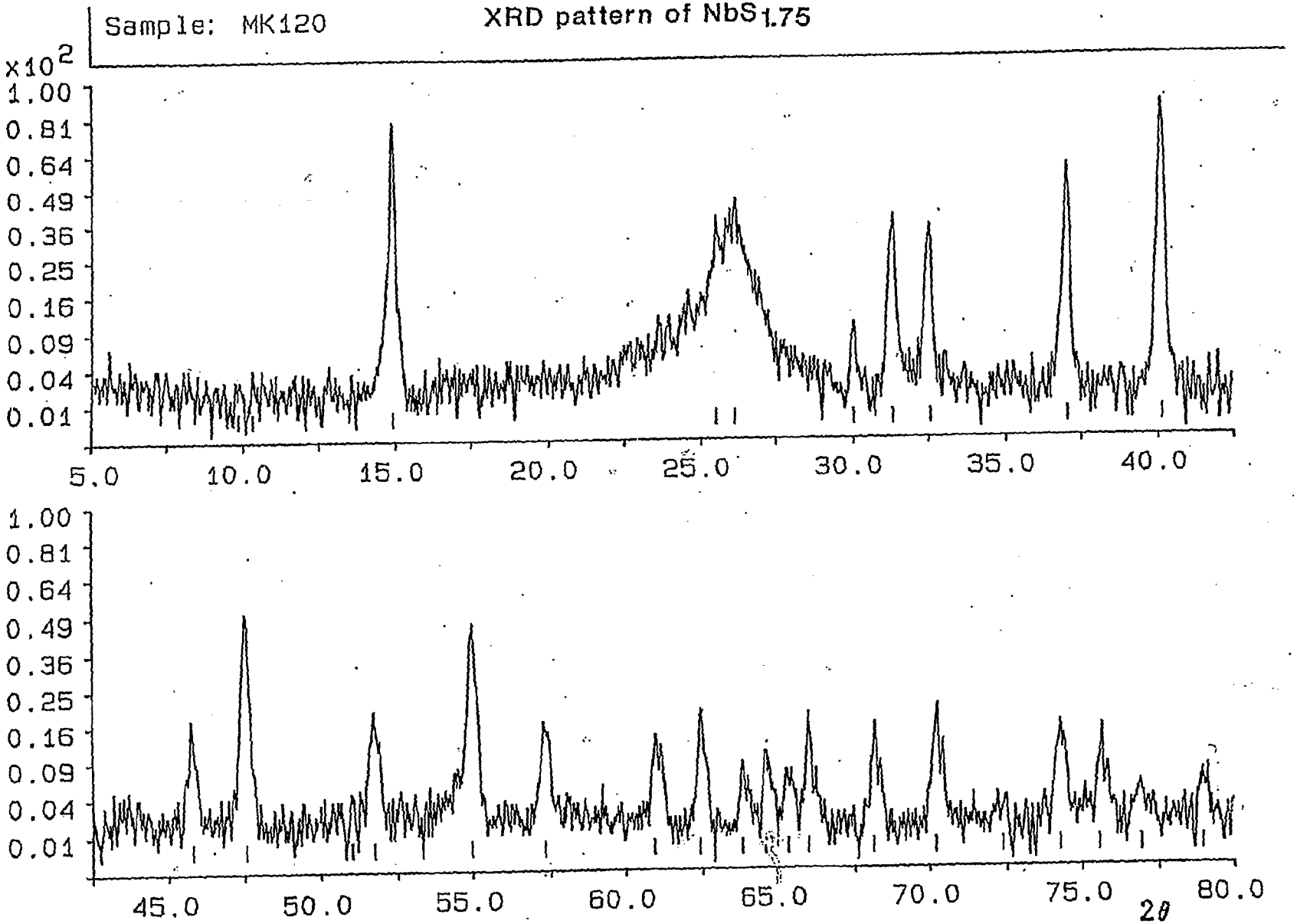

U.S. DEPARTMENT OF COMMERCE
Technology Administration
National Technical Information Service
Springfield, VA 22161 (703) 605-6000